



Effect of Large-Scale Mining Drainage on Groundwater Hydrogeochemical Evolution in Semi-Arid and Arid Regions

Ankun Luo^{1,2,3}, Guangcai Wang¹, Shuning Dong^{2,3}, Hao Wang^{2,3}, Zheming Shi^{1*}, Zhongkui Ji^{2,3} and Jiankun Xue^{2,3}

¹Key Laboratory of Groundwater Conservation of MWR, China University of Geosciences, Beijing, China, ²Xi'an Research Institute of China Coal Technology and Engineering Group Corp, Xi'an, China, ³Shaanxi Key Laboratory of Prevention and Control Technology for Coal Mine Water Hazard, Xi'an, China

OPEN ACCESS

Edited by:

Yong Xiao,
Southwest Jiaotong University, China

Reviewed by:

Lishuang Guo,
Ministry of Emergency Management,
China
Zhi Chen,
China Earthquake Administration,
China

*Correspondence:

Zheming Shi
szm@cugb.edu.cn

Specialty section:

This article was submitted to
Freshwater Science,
a section of the journal
Frontiers in Environmental Science

Received: 23 April 2022

Accepted: 13 May 2022

Published: 21 June 2022

Citation:

Luo A, Wang G, Dong S, Wang H,
Shi Z, Ji Z and Xue J (2022) Effect of
Large-Scale Mining Drainage on
Groundwater Hydrogeochemical
Evolution in Semi-Arid and
Arid Regions.
Front. Environ. Sci. 10:926866.
doi: 10.3389/fenvs.2022.926866

Groundwater evolution and circulation in coal mining areas will be significantly affected by natural processes and human activities. However, the impacts of large-scale mining drainage on groundwater hydrochemistry are unclear in the semi-arid and arid inland coalfields in northwest China. In particular, for shallow buried areas, the spontaneous combustion of coal seam outcrops forms burnt rock that is rich in fractures. Being a strong water-yield aquifer after receiving recharge, burnt rock has become a potential source of mine water inrush hazards. Therefore, drainage from this aquifer is necessary to eliminate potential hazards, which also leads to the deterioration of the local ecological diversity and sustainability. The hydrogeochemical method is an effective way to study the source and evolution of groundwater in mining areas and to determine the long-term cumulative effect of mining and drainage on the hydrogeochemical evolution of burnt rock areas. It is, however, still poorly understood. In this study, we employed the hydrochemical and isotope (²H, ³H, and ¹⁸O) to investigate the long-term effects of drainage on the hydrogeochemical evolution in the coalfield of southern Xinjiang, China. The results showed that the hydrochemical environment became more complex as the effect of recharge of different tritium-based groundwater ages in multiple-layered aquifer system and leads to the changes in the concentration of the chemical components. Before large-scale mining drainage, groundwater flowed from west to east and was finally discharged into the Kuqa River. The major water-rock interactions that occurred were the dissolution of halite, carbonate and gypsum dissolution, cation exchange, and dedolomitization. After large-scale and long-term mining drainage from the burnt rock aquifer, the groundwater flow field had changed, and the Kuqa river turned to recharge into the burnt rock aquifer, the hydrochemical evolution also changed from water-rock interaction to mixture. This was caused by the significant decline in the groundwater level and changes in groundwater circulation in the mining area, which further led to the loss of valuable surface water resources in this arid area. Based on the characteristics and recharge conditions of burnt rock, we suggested that grouting can effectively cut off the hydraulic connection between the river and burnt rock and thus protect water resources.

Keywords: groundwater, large-scale mining drainage, burnt rock aquifer, hydrogeochemistry, semi-arid and arid regions

INTRODUCTION

Spontaneous combustion is commonly observed in coal seam outcrops all around the world (Oren and Sensogut, 2010; Song et al., 2017; Kruszcwski et al., 2018; Onifade and Genc, 2018; Zhang et al., 2020). During spontaneous combustion, heat spreads upwards, which causes the overlying rocks to heat up and transform into a suite of thermally metamorphosed rocks (named burnt rock) through a process known as combustion metamorphism (Shi et al., 2021). As a result, the color and structure of the burnt rock change significantly (Huang et al., 2008) and eventually turn reddish and rich in fractures. Previous studies have mostly focused on the petrology and mineralogy of burnt rocks to describe mineral and textural transformations during spontaneous combustion (Baboolal et al., 2018; Laita et al., 2019). However, the burnt rock becomes a strong water-yield aquifer after receiving recharge due to fractures created by the combustion metamorphism processes, affecting the safety of the underground coal mining process. In northwest China, burnt rocks are widely formed in the coal outcrop area as the shallow buried Jurassic strata (Ma et al., 2021). Yuan et al. (2019) have documented that the structure of the burnt rock is damaged with a large number of pores and fractures, which is one of the key factors of instability in the surrounding rock. Xue et al. (2021) employed the AHP and entropy-weight method to evaluate the water abundance of BRA and to avoid the recurrence of water inrush during coal mining. Because of the strong water yield, a water inrush from BRA occurred in the underground coal mine of Yongxin, causing a tunnel flooding incident that killed two people (Xue et al., 2021). In order to avoid such hazards, it is necessary to drain water from the overlying aquifer before mining (Dong et al., 2021). Secondary problems such as groundwater pollution (Wang et al., 2021b), ground subsidence (Zeng et al., 2020), and soil salinization (Zhang et al., 2007) may also occur. Furthermore, excessive drainage may change the flow path of the groundwater (Dimitrova-Petrova et al., 2020), which can complicate the hydrogeological condition of the mining area. The hydrogeochemical process and evolution of groundwater can reflect the flow process (Carrillo-Rivera et al., 2007; Xiao et al., 2022a), and the hydrogeochemical characteristics can change significantly in the mining area after excessive drainage. Therefore, it is necessary to study the hydrogeochemistry of BRA under the influence of large-scale mining drainage, which is poorly understood.

The hydrochemical and stable isotope analysis can be used to investigate the groundwater circulation, hydraulic connection, and water–rock interaction (Keita and Tang, 2017; Emvoutou et al., 2018; Meyzonnat et al., 2021). By combining the Piper diagram, Durov plot, and Gibbs plot, groundwater hydrogeochemical processes can be studied (Salameh et al., 2018). Stable isotopes and radioactive isotopes are used to identify the source and age of groundwater (Huang et al., 2017; Wang et al., 2021a). With the help of multivariate statistical analysis (MSA), such as hierarchical cluster analysis (HCA) (Barzegar et al., 2017), principal component analysis (PCA) (Dehghanzadeh et al., 2015; Xiao et al., 2022b), and correlation analysis (CA) (Qiao

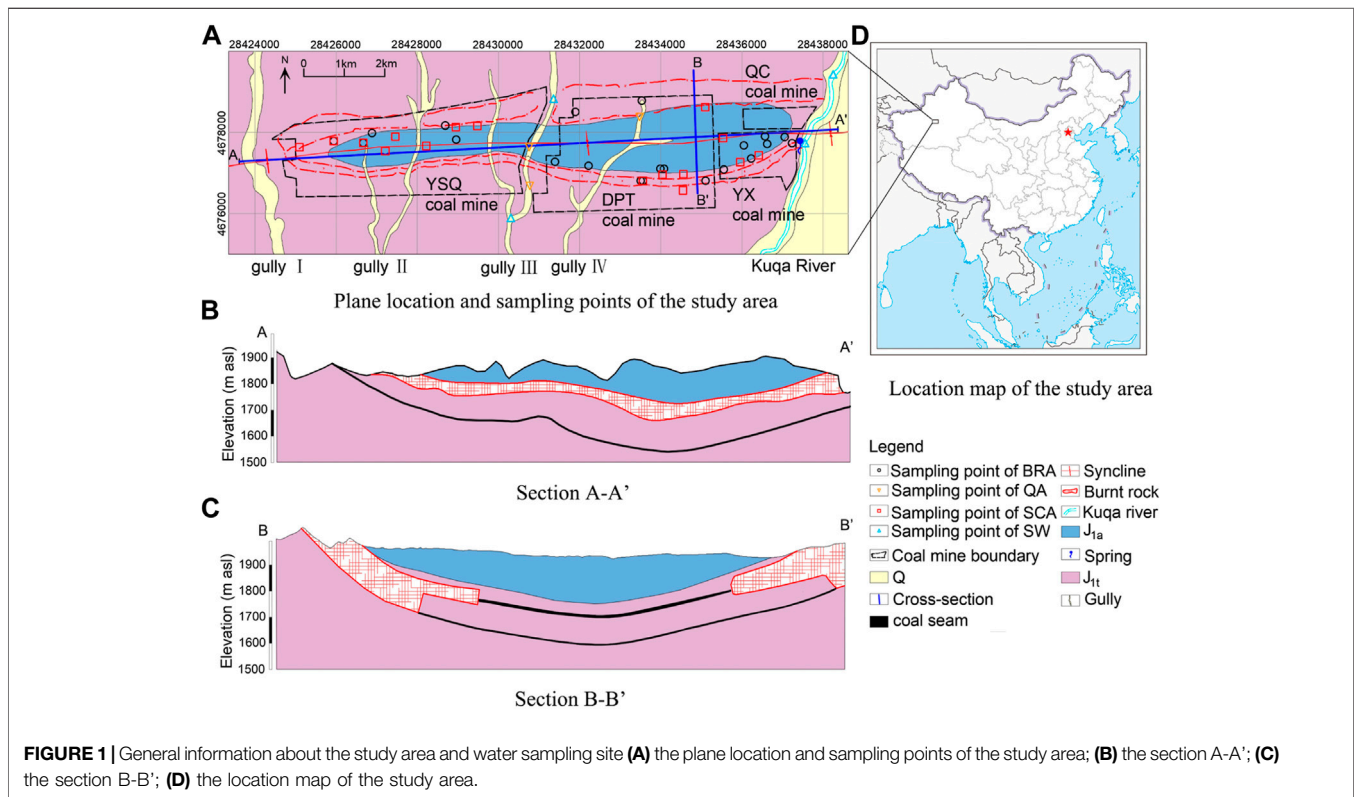
et al., 2019), a more reasonable explanation for the hydrogeochemical changes can be obtained (Qu et al., 2021).

In this study, the integration of hydrogeochemistry and isotope (^2H , ^{18}O , and ^3H) analysis, MSA, hydrogeological condition, and coal mine exploitation was employed to identify the origins of groundwater and hydrogeochemical evolution under the influence of mining drainage in a typical arid coalfield located in southern Xinjiang that is affected by BRA in China. This work aimed to 1) identify the key factors controlling hydrogeochemical origin and evolution, 2) reveal the effect of large-scale mining drainage on the hydrogeochemistry for BRA in the coalfield, and 3) propose reasonable suggestions for water resource protection and mine safety production.

STUDY AREA

The A-ai coalfield is located in southern Xinjiang, China (Figure 1), which has a total area of 32 km². It is dominated by a continental arid climate, characterized by strong evaporation, low precipitation, and frequent droughts (Sabit et al., 2008), with an average annual precipitation of 90.09 mm and mean annual pan evaporation of 2,219 mm. Approximately, 85% of the annual precipitation occurs between June and September (Li et al., 2011). The landform is influenced by wind erosion with surface elevations varying from +1840 m to +2005 m, and the topography of the A-ai coalfield is generally a basin with high surroundings and a low middle. In addition, four gullies are perpendicular to this basin from the north to the south. The Kuqa River is the only perennial river in the region that acts as the main source of drinking water. A syncline runs through this area and stretches 12 km wide from west to east and has a length of 2–4 km from south to north. No other large faults are found here. The coal seam spreads along the two wings of the syncline and is exposed on the surface. Due to the subsurface spontaneous combustion of the coal seam, sandstone and mudstone on the roof have changed the appearance and petrologic characters into burnt rock with a great number of fractures (Figure 2). Therefore, the A-ai coalfield is bounded by gully I in the west, the Kuqa river in the east, and the coal seam and burnt rock outcrop in the north and south (Figure 1).

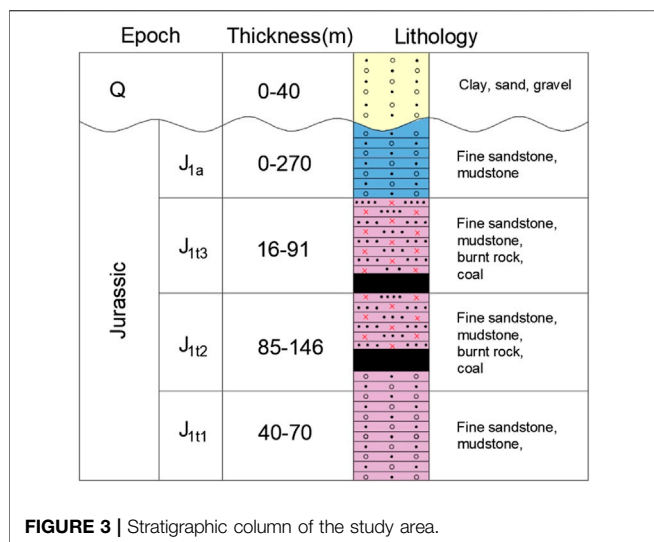
The sedimentary sequence above coal-bearing strata in the study area is shown in Figure 3. From top to bottom, the strata are Quaternary and Jurassic. According to the microscopic features of typical samples from Jurassic, quartz, feldspar, mica, carbonate, and gypsum account for more than 90% (Liu et al., 2011). The quaternary aquifer (QA) is only deposited near gullies and the Kuqa river and has a thickness of 0–40 m. The Jurassic Ahe Group (J_{1a}) is dominated by fine sandstone and mudstone but is poor in water. The Jurassic Taliqike Group (J_{1t}) is the coal-bearing stratum, and above the coal seam is a sandstone confined aquifer (SCA). In the coal outcrop areas, the overlying rock of the coal seam gradually turns to melted or honeycombed forms, generating plenty of cracks and fractures during the



combustion of coal. Burnt rocks can easily receive recharges from precipitation and become a strong water-yield aquifer. The drilling unit water inflow (q) is a generally accepted index in China to evaluate the water yield of an aquifer (Qiao et al., 2017). According to the pumping test, the average hydraulic conductivity (K) and q value (flow rate when the water level drops 10 m for a 91 mm borehole) of the SCA are 0.049 m/d and 0.017 L/(sm), respectively, indicating a weak permeability and water yield. Therefore, this aquifer has little impact on coal mining. In contrast, the burnt rock aquifer (BRA) is distributed at the outcrops of coal seams on both sides of the syncline with great permeability and a very strong wateryield

(with an average K of 17.874 m/d and q of 11.434 L/(sm), indicating that BRA is the main water-filled aquifer and the primary threat to coal mining safety. Under natural conditions or before large-scale coal mining, the groundwater recharge sources are precipitation and surface water (SW) from gullies in the rainy season. The direction of groundwater flow is from the west to the east, which then gets discharged to the Kuqa River in the east in the form of spring and direct contact.

Four coal mines are distributed in this area, namely, Yushuquan (YSQ), Dapingtan (DPT), Yongxin (YX), and Qiuci (QC). From 2012 to 2014, due to the production of new mines and upgrades in the mining technology (from the



pillar mining method to the comprehensive mechanized mining method), the amount of coal production increased sharply from 0.12 to 1.59 million tons per year and has since been maintained to date. Several water inrush disasters have occurred in this area, causing the deaths of 10 people and the flooding of several tunnels in the A-ai coalfield. Therefore, with an increase in mining output, the large-scale drainage of BRA has been carried out by drilling holes in an effort to avoid disasters such as that which occurred in 2015.

MATERIAL AND METHODS

Groundwater Sampling and Analytical Techniques

In this study, 46 water samples from groundwater and surface water were obtained from the A-ai coalfield from the years 2007–2021. The data included 22 samples from the BRA (including 1 sample from the spring), 17 samples from the SCA, 3 samples from QA, and 4 samples from SW (2 samples from the Kuqa river and 2 samples from the gully III). Sampling locations were recorded using a portable GPS device and displayed in **Figure 1**. All of the groundwater samples were taken from springs or boreholes. Water samples were mainly analyzed at the Shaanxi Key Laboratory of Prevention and Control Technology for Coal Mine Water Hazard. The concentrations of $\text{Na}^+ + \text{K}^+$, Mg^{2+} , Ca^{2+} , SO_4^{2-} , and Cl^- ions were measured by ion chromatography, while the concentrations of HCO_3^- and CO_3^{2-} were measured by the traditional titrimetric method. The total dissolved solids (TDS) were calculated based on all the ion concentrations determined previously (**Table 1**). pH was measured *in situ* with a portable pH meter, and tritium (^3H) was determined on electrolytically enriched water samples by liquid scintillation spectrometry. For the reliability of the chemical data (Chen et al., 2015), the error of the charge balance error (CBE) was calculated as follows:

$$\text{CBE} = \frac{|\sum \text{cations} - \sum \text{anions}|}{|\sum \text{cations} + \sum \text{anions}|} \times 100,$$

where all ions are measured in meq/L. The calculated results of the CBE showed that the uncertainty was less than $\pm 5\%$, which is acceptable for this study. The stable isotopes of $\delta^{18}\text{O}$ and $\delta^2\text{H}$ were measured by using a liquid water isotope analyzer (LGR LWIA-24d) and compared with the Vienna standard mean ocean water standard, which had precisions of 0.21‰ and 0.04‰, respectively.

Pumping tests were conducted to obtain the aquifer hydraulic conductivity. A total of 10 single-hole steady-flow pumping tests were carried out in the study area in the past 10 years.

Multivariate Statistical Analysis

Multivariate statistical analysis has been widely used to extract valuable information from large hydrogeochemical datasets (Khanoranga and Khalid, 2019; Liu et al., 2020). In this study, hierarchical cluster analysis (HCA), principal component analysis (PCA), and correlation analysis (CA) were employed to analyze the hydrogeochemical classification and the temporal and spatial variation. The Ward linkage method and the Euclidean distance were performed in the HCA of this study, and a dendrogram was used to graphically show clusters of the datasets and their proximity (Cloutier et al., 2008). PCA is used to explain the majority of variance by extracting the eigenvalues from the correlation between the chemical variables (Singh et al., 2017), while CA can reveal a statistical relationship between two or more variables (Nagaraju et al., 2016). All statistical calculations were performed in SPSS software version 20.0 for Windows.

RESULTS

General Hydrogeochemical Properties

The variation of hydrogeochemical composition in coalfields is affected by many factors, such as hydrogeological condition, lithology, mineral composition, precipitation, temperature, and also by mining and other human activities (Zhang et al., 2021). In **Table 1**, all the water samples were classified by the sampling location and arranged by the sampling time. The pH of all samples ranged from 7.11 to 8.88, with a mean of 7.82, which is slightly alkaline. It was closely related to alkaline mineral sources in the aquifer system, especially samples 40 and 41 from the Kuqa River (8 and 8.19, respectively) indicating the close relationship with soil salinization (Xuemei et al., 2009). The TDS reflects the strength of water–rock interaction and the hydraulic connection between multi-aquifers (Shvartsev et al., 2016; Hao et al., 2020). The TDS values of BRA ranged from 505.53 mg/L to 2,124.90 mg/L with a mean of 1570.23 mg/L, while those of SCA ranged from 1394.93 mg/L to 7058.26 mg/L with a mean of 3331.89 mg/L. The ion concentrations in both BRA and SCA were all obviously larger than those in SW and QA. Since the

TABLE 1 | Hydrogeochemical data from the study area.

| No. | Year | Sample location | Ca ²⁺ (mg/L) | Mg ²⁺ (mg/L) | Na ⁺ +K ⁺ (mg/L) | HCO ₃ ⁻ (mg/L) | SO ₄ ²⁻ (mg/L) | Cl ⁻ (mg/L) | Water chemical type | TDS (mg/L) | pH | CBE | ³ H (TU) | δD | δ ¹⁸ O | SI _{Calcite} | SI _{Dolomite} | SI _{Gypsum} | SI _{Halite} |
|-----|------|-----------------|-------------------------|-------------------------|--|--------------------------------------|--------------------------------------|------------------------|--|------------|------|--------|---------------------|--------|-------------------|-----------------------|------------------------|----------------------|----------------------|
| 1 | 2007 | Spring | 147.13 | 73.19 | 442.96 | 233.4 | 496.27 | 640.94 | Na-Cl-SO ₄ | 1928.83 | - | -1.77% | - | - | - | - | - | - | - |
| 2 | 2010 | BRA | 131.34 | 76.40 | 509.52 | 378.87 | 554.70 | 611.03 | Na-Cl-SO ₄ | 2072.43 | 7.40 | -2.56% | - | -56.44 | -9.12 | 0.38 | 0.81 | -0.96 | -5.15 |
| 3 | 2010 | BRA | 115.49 | 59.09 | 358.32 | 301.62 | 409.85 | 451.23 | Na-Cl-SO ₄ | 1544.79 | 7.70 | -2.39% | - | -54.12 | -8.74 | 0.57 | 1.13 | -1.07 | -5.42 |
| 4 | 2011 | BRA | 92.02 | 32.01 | 472.17 | 347.72 | 430.43 | 433.39 | Na-Cl-SO ₄ | 1659.99 | - | -1.42% | 8.96 | -55.4 | -7.45 | - | - | - | - |
| 5 | 2011 | BRA | 106.05 | 67.07 | 362.39 | 297.29 | 403.27 | 446.80 | Na-Mg-Ca-Cl-SO ₄ | 1555.12 | - | -1.06% | 3.03 | -61.8 | -8.23 | - | - | - | - |
| 6 | 2011 | BRA | 87.53 | 64.01 | 279.52 | 233.58 | 346.48 | 368.61 | Na-Cl-SO ₄ | 1273.38 | - | -1.43% | 5.54 | -58.4 | -8.15 | - | - | - | - |
| 7 | 2011 | BRA | 87.53 | 53.46 | 271.49 | 201.73 | 348.95 | 356.32 | Na-Cl-SO ₄ | 1229.06 | - | -2.43% | - | -57.7 | -8.29 | - | - | - | - |
| 8 | 2012 | BRA | 158.72 | 70.89 | 492.82 | 296.01 | 620.95 | 627.64 | Na-Cl-SO ₄ | 2,124.90 | - | -2.88% | - | - | - | - | - | - | - |
| 9 | 2012 | BRA | 136.67 | 98.98 | 479.04 | 277.89 | 564.99 | 638.28 | Na-Cl-SO ₄ | 2,108.84 | 7.90 | -0.24% | - | - | - | 0.75 | 1.65 | -0.94 | -5.16 |
| 10 | 2012 | BRA | 123.45 | 38.79 | 495.67 | 187.27 | 446.89 | 670.19 | Na-Cl-SO ₄ | 1876.13 | - | -3.42% | - | - | - | - | - | - | - |
| 11 | 2012 | BRA | 114.63 | 58.85 | 287.07 | 241.64 | 373.23 | 378.71 | Na-Ca-Cl-SO ₄ | 1823.45 | 7.90 | -0.78% | - | - | - | 0.69 | 1.36 | -1.08 | -5.58 |
| 12 | 2012 | BRA | 98.89 | 61.58 | 357.68 | 251.63 | 400.58 | 411.00 | Na-Cl-SO ₄ | 1455.55 | 7.84 | 0.56% | - | - | - | 0.57 | 1.22 | -1.13 | -5.46 |
| 13 | 2012 | BRA | 92.58 | 52.17 | 292.53 | 193.31 | 346.89 | 404.24 | Na-Cl-SO ₄ | 1288.20 | - | -2.73% | - | - | - | - | - | - | - |
| 14 | 2018 | BRA | 127 | 62.66 | 370.62 | 317.18 | 433.44 | 429.14 | Na-Cl-SO ₄ | 1581.45 | 7.6 | 0.03% | - | - | - | 0.53 | 1.03 | -1.02 | -5.43 |
| 15 | 2019 | BRA | 89.06 | 54 | 479.77 | 376.44 | 443.01 | 450.03 | Na-Cl-SO ₄ | 1704.09 | 7.75 | 0.02% | - | - | - | 0.59 | 1.24 | -1.16 | -5.3 |
| 16 | 2019 | BRA | 135.83 | 64.72 | 379.43 | 331.28 | 424.46 | 453.06 | Na-Cl-SO ₄ | 1630.46 | 8.05 | 0.48% | - | - | - | 1.01 | 1.98 | -1.01 | -5.39 |
| 17 | 2020 | BRA | 118.53 | 93.66 | 385.44 | 423.67 | 485.72 | 453.36 | Na-Mg-Cl-SO ₄ | 1758.06 | 8.77 | -1.33% | - | - | - | 1.66 | 3.52 | -1.06 | -5.39 |
| 18 | 2020 | BRA | 124.95 | 80.81 | 369.49 | 380.63 | 486.77 | 463.96 | Na-Cl-SO ₄ | 1716.30 | 7.91 | -3.10% | - | - | - | 0.88 | 1.86 | -1.00 | -5.4 |
| 19 | 2020 | BRA | 55.03 | 31.81 | 426.03 | 435.83 | 263.78 | 346.47 | Na-Cl-HCO ₃ | 1341.04 | 7.8 | 0.09% | - | - | - | 0.54 | 1.12 | -1.51 | -5.45 |
| 20 | 2021 | BRA | 95.38 | 66.37 | 493.69 | 347.37 | 467.98 | 439.78 | Na-Cl-SO ₄ | 1736.89 | 7.75 | 3.71% | - | - | - | 0.51 | 1.07 | -1.1 | -5.29 |
| 21 | 2021 | BRA | 46.94 | 31.89 | 137.64 | 219.92 | 231.79 | 72.49 | Na-Mg-SO ₄ -HCO ₃ | 630.71 | 7.87 | 0.01% | - | - | - | 0.32 | 0.75 | -1.51 | -6.59 |
| 22 | 2021 | BRA | 61.9 | 30.4 | 72.17 | 176.71 | 191.00 | 61.7 | Na-Ca-Mg-SO ₄ -HCO ₃ | 505.53 | 7.84 | -0.76% | - | -56.73 | -8.96 | 0.34 | 0.65 | -1.45 | -6.93 |
| 23 | 2007 | SCA | 107.84 | 52.95 | 633.12 | 248.66 | 632.89 | 675.51 | Na-Cl-SO ₄ | 2,255.48 | - | -1.70% | - | - | - | - | - | - | - |
| 24 | 2007 | SCA | 145.33 | 53.03 | 552.78 | 184.95 | 656.75 | 671.68 | Na-Cl-SO ₄ | 2,172.05 | - | -2.73% | - | - | - | - | - | - | - |
| 25 | 2010 | SCA | 76.36 | 45.48 | 2,580.23 | 163.11 | 373.64 | 3893.51 | Na-Cl | 7058.26 | - | -4.06% | - | - | - | - | - | - | - |
| 26 | 2010 | SCA | 235.51 | 134.66 | 704.67 | 423.36 | 938.22 | 957.14 | Na-Cl-SO ₄ | 3181.88 | 7.20 | -2.30% | 0.36 | -55.34 | -8.9 | 0.4 | 0.84 | -0.62 | -4.84 |
| 27 | 2010 | SCA | 233.71 | 141.25 | 591.33 | 373.69 | 889.66 | 863.13 | Na-Cl-SO ₄ | 2,905.93 | 7.20 | -2.10% | 0.34 | -54.36 | -8.67 | 0.36 | 0.78 | -0.63 | -4.96 |
| 28 | 2010 | SCA | 122.28 | 53.59 | 484.38 | 323.16 | 497.92 | 564.03 | Na-Cl-SO ₄ | 1883.78 | 7.30 | -2.70% | 0.39 | -56 | -9.03 | 0.2 | 0.32 | -1.00 | -5.2 |
| 29 | 2010 | SCA | 133.61 | 67.33 | 424.14 | 670.98 | 457.59 | 358.93 | Na-HCO ₃ -Cl-SO ₄ | 1777.09 | 7.50 | -2.43% | 0.28 | -56.77 | -8.87 | 0.75 | 1.47 | -1.01 | -5.45 |
| 30 | 2011 | SCA | 85.85 | 43.58 | 618.56 | 156.61 | 337.43 | 880.19 | Na-Cl | 2054.36 | - | -2.64% | - | -60.1 | -8.84 | - | - | - | - |
| 31 | 2012 | SCA | 132.66 | 72.45 | 653.96 | 415.48 | 705.88 | 580.68 | Na-Cl-SO ₄ | 2,353.37 | 7.43 | 1.15% | - | - | - | 0.43 | 0.87 | -0.88 | -5.07 |
| 32 | 2018 | SCA | 154.47 | 158.98 | 1431.09 | 846.14 | 56.1 | 2,233.79 | Na-Cl | 4457.50 | 7.39 | 0.06% | - | - | - | 0.72 | 1.75 | -2.05 | -4.18 |
| 33 | 2019 | SCA | 232.28 | 149 | 566.06 | 289.43 | 717.3 | 951.38 | Na-Mg-Ca-Cl-SO ₄ | 2,760.74 | 7.48 | 0.03% | - | - | - | 0.54 | 1.17 | -0.71 | -4.93 |
| 34 | 2019 | SCA | 139.78 | 71.11 | 757.42 | 430.92 | 821.48 | 672.71 | Na-Cl | 2,677.96 | 7.43 | 0.01% | - | - | - | 0.44 | 0.86 | -0.83 | -4.95 |
| 35 | 2020 | SCA | 29.23 | 14.6 | 2077.98 | 1161.08 | 41.22 | 2,201.75 | Na-Cl | 5059.17 | 8.38 | 2.31% | - | - | - | 1.07 | 2.15 | -2.89 | -4.03 |
| 36 | 2020 | SCA | 227.75 | 114.43 | 1158.29 | 288.65 | 976.07 | 1492.13 | Na-Cl-SO ₄ | 4113.00 | 7.22 | 0.03% | - | - | - | 0.22 | 0.42 | -0.65 | -4.45 |
| 37 | 2020 | SCA | 92.28 | 90.47 | 858.5 | 648.08 | 85.5 | 1291.08 | Na-Cl-HCO ₃ | 2,754.24 | 8.48 | -2.49% | - | - | - | 1.49 | 3.27 | -1.96 | -4.61 |
| 38 | 2021 | SCA | 60.53 | 50.56 | 2,512.05 | 668.41 | 1104.56 | 2,905.7 | Na-Cl | 6967.61 | 8.15 | -3.65% | - | - | - | 0.85 | 1.9 | -1.27 | -3.85 |
| 39 | 2021 | SCA | 98.98 | 66.48 | 1315.96 | 486.07 | 1253.95 | 1168.27 | Na-Cl-SO ₄ | 4146.68 | 7.72 | -3.03% | - | - | - | 0.55 | 1.21 | -0.9 | -4.5 |
| 40 | 2012 | | 48.5 | 24.08 | 8.71 | 120.82 | 62.14 | 55.32 | | 259.16 | 8 | -0.82% | 10.37 | -46.9 | -7.36 | 0.31 | 0.59 | -1.93 | -7.87 |

(Continued on following page)

TABLE 1 | (Continued) Hydrogeochemical data from the study area.

| No. | Year | Sample location | Ca ²⁺ (mg/L) | Mg ²⁺ (mg/L) | Na ⁺ +K ⁺ (mg/L) | HCO ₃ ⁻ (mg/L) | SO ₄ ²⁻ (mg/L) | Cl ⁻ (mg/L) | Water chemical type | TDS (mg/L) | pH | CBE | ³ H (TU) | δD | δ ¹⁸ O | SI _{calcite} | SI _{dolomite} | SI _{gypsum} | SI _{halite} |
|-----|------|-----------------|-------------------------|-------------------------|--|--------------------------------------|--------------------------------------|------------------------|--|------------|------|--------|---------------------|--------|-------------------|-----------------------|------------------------|----------------------|----------------------|
| | | Kuqa River | | | | | | | Ca-Mg-HCO ₃ ⁻ | | | | | | | | | | |
| 41 | 2021 | Kuqa River | 79.9 | 28.6 | 33.14 | 185.91 | 170 | 43.1 | Ca-Mg-SO ₄ ⁻ | 447.70 | 8.19 | -0.83% | - | -54.04 | -8.22 | 0.82 | 1.47 | -1.38 | -7.42 |
| 42 | 2011 | Gully III | 91.06 | 29.74 | 31.26 | 149.07 | 201.64 | 55.53 | Ca-Mg-SO ₄ ⁻ | 488.03 | - | 0.26% | 7.11 | -54.2 | -6.52 | - | - | - | - |
| 43 | 2021 | Gully III | 52.62 | 39.89 | 102.01 | 200.51 | 215.46 | 78.69 | Na-Mg-Ca-SO ₄ -HCO ₃ | 588.93 | 7.55 | 0.01% | - | - | - | 0.02 | 0.2 | -1.49 | -6.68 |
| 44 | 2012 | QA | 77.94 | 44.12 | 230.83 | 239.3 | 178.86 | 316.74 | Na-Cl | 968.14 | 8.26 | 0.57% | - | - | - | 0.92 | 1.88 | -1.48 | -5.74 |
| 45 | 2012 | QA | 99.20 | 65.54 | 124.69 | 223.52 | 302.04 | 212.76 | Na-Mg-Ca-SO ₄ -Cl | 924.60 | - | -1.94% | - | - | - | - | - | - | - |
| 46 | 2012 | QA | 39.68 | 32.10 | 177.01 | 144.98 | 241.55 | 191.48 | Na-Cl-SO ₄ | 764.47 | - | -4.47% | - | - | - | - | - | - | - |

spontaneous combustion of coal seams leads to a significant increase in the fractures in BRA, there will be a good hydraulic connection and thus lead to a small standard deviation in the ion concentrations, the TDS, and pH in the aquifer.

Figure 4 shows that several main hydrogeochemical types could be identified in all samples. The water samples from BRA and SCA showed a similar hydrogeochemical type but were different in mineralization. SCA samples were presented as a highly saline Na-Cl-SO₄ type. Although the major hydrogeochemical type in SCA was dominated by Na-Cl-SO₄, the average concentration of SO₄ was just slightly excess 25%, while the concentrations of both Na and Cl exceeded 55%. Meanwhile, the standard deviation of TDS in SCA was 1667.68 mg/L, which gives an indication of the heterogeneity. A total of 22 water samples from BRA are Na-Cl-SO₄ water chemical type with a lower TDS, including a sample from the spring near the Kuqa River (the spring is origin from the BRA at a flow rate of 0.69 L/s in 2007 but stopped flowing in 2015, when large-scale mining drainage began). In contrast, mixed water chemical types were observed in samples from the surface water and QA with low mineralization (ranging from 259.16 to 968.14 with a mean of 634.43). As a local drinking water source, two samples from the Kuqa River over 10 years met the WHO guidelines for both drinking and irrigation. The samples of QA were collected from different gullies with the weak hydraulic connections.

Relationships Among Major Ions by Multivariate Statistical Analysis

Six major ions were classified by the R-mode HCA process, while the Ward method and squared Euclidian distances were employed to measure the similarity between them. As shown in Figure 5, these ions could be classified into two clusters. Ca, Mg, SO₄, and HCO₃ were classified into cluster I, suggesting the dissolution of carbonate. Cluster comprised Na and Cl, indicating the dissolution of halite.

The Pearson correlation coefficients are presented in Table 2, which shows that the TDS correlates strongly with Cl and Na (greater than 0.9), indicating that the dissolution of halite plays an important role in the increment of TDS. In addition, Ca correlated strongly with Mg (0.846), indicating the dissolution of dolomite.

We further used the principal component analysis to investigate the hydrochemical processes in this area. The principal components were extracted from the correlation matrix from the seven parameters (Ca, Mg, Na, HCO₃, SO₄, Cl, and TDS). The Kaiser criterion is such that only the components with eigenvalues greater than one are retained (Yilmaz and Buyukyildiz, 2015). Table 3 shows the principal component loadings and their separate variances explained. The result shows that the first two components extracted have eigenvalues greater than one and account for 80.61% of the total variance in the dataset. Component 1 is characterized by highly positive loadings in Na, Cl, and TDS (all higher than 0.9) with 52.28% of the explained variance. Component 2 is characterized by highly positive loadings in Ca, Mg, and SO₄. The loadings of the chemical parameters can be defined by descriptive terms according to the position in the plane

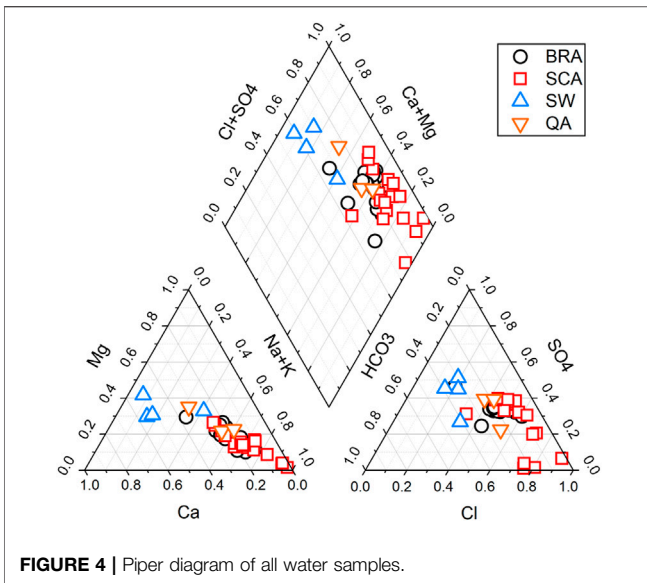


FIGURE 4 | Piper diagram of all water samples.

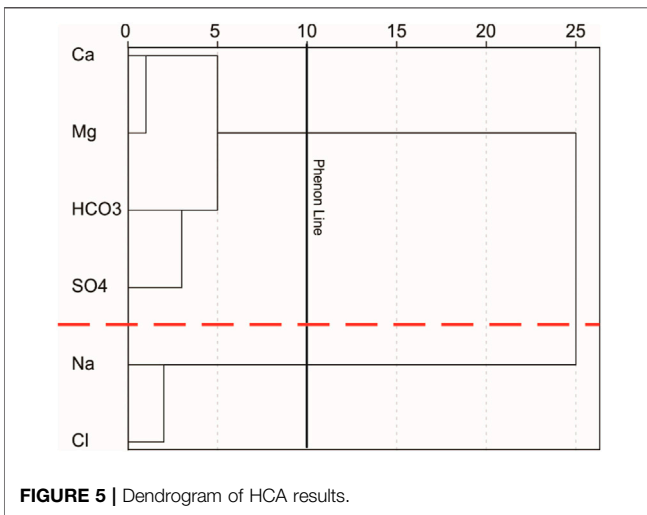


FIGURE 5 | Dendrogram of HCA results.

(Figure 6). Component 1 was defined as the salinity component because of the close relationship of Na, Cl, and TDS, while component 2 was defined as the hardness component because of the association of Ca and Mg, which was used to calculate hardness. The factors that cause these high loads will be discussed in a later section.

The results of the multivariate statistical methods (HCA, PCA, and CA), Na, Cl, and TDS are dominant in cluster 1 and those of Ca, Mg, and SO₄ are dominant in cluster 2. This means that the natural processes dominate the evolution of groundwater hydrogeochemistry in this study.

Relationship Between the Hydraulic Conductivity and TDS

The hydraulic conductivity K can reflect the residence time by affecting the seepage velocity (Loaiciga, 2004), while the

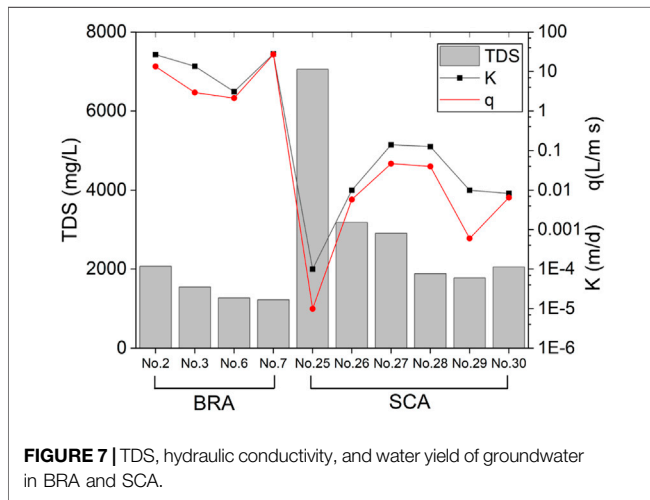
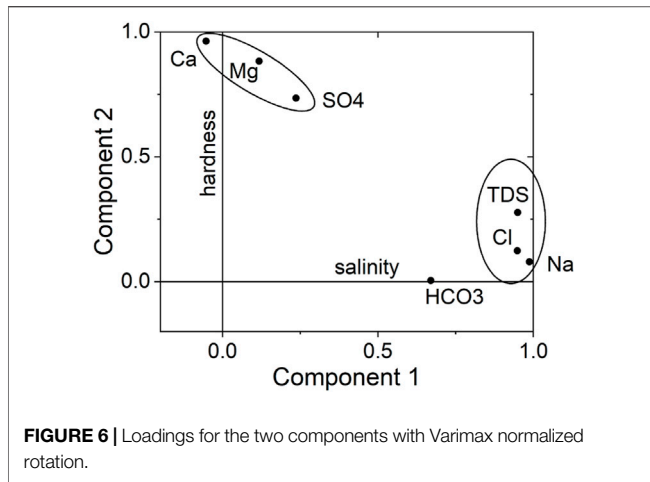
TABLE 2 | Pearson correlation matrix of the major chemical parameters in groundwater.

| | Ca | Mg | Na | HCO ₃ | SO ₄ | Cl | TDS |
|------------------|----|----------------|-------|------------------|-----------------|----------------|----------------|
| Ca | 1 | 0.846** | 0.019 | -0.004 | 0.597** | 0.087 | 0.212 |
| Mg | | 1 | 0.146 | 0.225 | 0.439** | 0.234 | 0.318* |
| Na | | | 1 | 0.568** | 0.334* | 0.970** | 0.978** |
| HCO ₃ | | | | 1 | 0.030 | 0.467** | 0.534** |
| SO ₄ | | | | | 1 | 0.249 | 0.466** |
| Cl | | | | | | 1 | 0.963** |
| TDS | | | | | | | 1 |

TABLE 3 | Principal component loadings and explained variance for two components.

| Parameter | Component 1 | Component 2 |
|--------------------------|--------------|--------------|
| Ca | -0.053 | 0.963 |
| Mg | 0.118 | 0.883 |
| Na | 0.987 | 0.079 |
| HCO ₃ | 0.670 | 0.004 |
| SO ₄ | 0.237 | 0.734 |
| Cl | 0.949 | 0.123 |
| TDS | 0.950 | 0.277 |
| Eigenvalue | 3.66 | 1.98 |
| Explained variance (%) | 52.28 | 28.33 |
| Cumulative % of variance | 52.28 | 80.61 |

length of residence time can reflect the degree of water–rock interaction, which causes changes in the characteristics of the hydrogeochemistry, especially TDS (Jia et al., 2019). Ten pumping tests were conducted to assess the hydraulic conductivity of BRA and SCA in the study area (Figure 7). The values of K and TDS in BRA ranged from 3.11 to 27.86 m/d and 505.53–2,121.90 mg/L, with averages of 17.874 m/d and 1570.23 mg/L, respectively. In contrast, the values of K and TDS in SCA ranged from 0.0001 to 0.14 m/d and 1394.93–7058.26 mg/L, with averages of 0.0049 m/d and 3331.89 mg/L, respectively. Similarly, the values of q in SCA ranged from 0.00001 to 0.047 L/(m s) with an average of 0.017 L/(m s), while the values of q in BRA ranged from 2.13 to 27.226 L/(m s) with an average of 11.434 L/(m s). Obviously, the K and q values of BRA are significantly larger than those of SCA, while the TDS is lower in BRA than in SCA. The pumping test in the three boreholes (including samples 2 and 26 from the same borehole but in different aquifers, and samples 3 and 28, 6 and 30), the difference are shown in K and TDS values of the two aquifers. The four water samples (samples 2 and 3 from BRA and samples 26 and 28 from SCA) showed the same water chemical type but with difference in mineralization, while two samples (samples 6 and 30) from these two aquifers showed different chemical types. In addition, sample 25 showed the highest TDS but the lowest K. Under the same hydraulic gradient, the smaller value of K provided more sufficient residence time and a wider range of water–rock



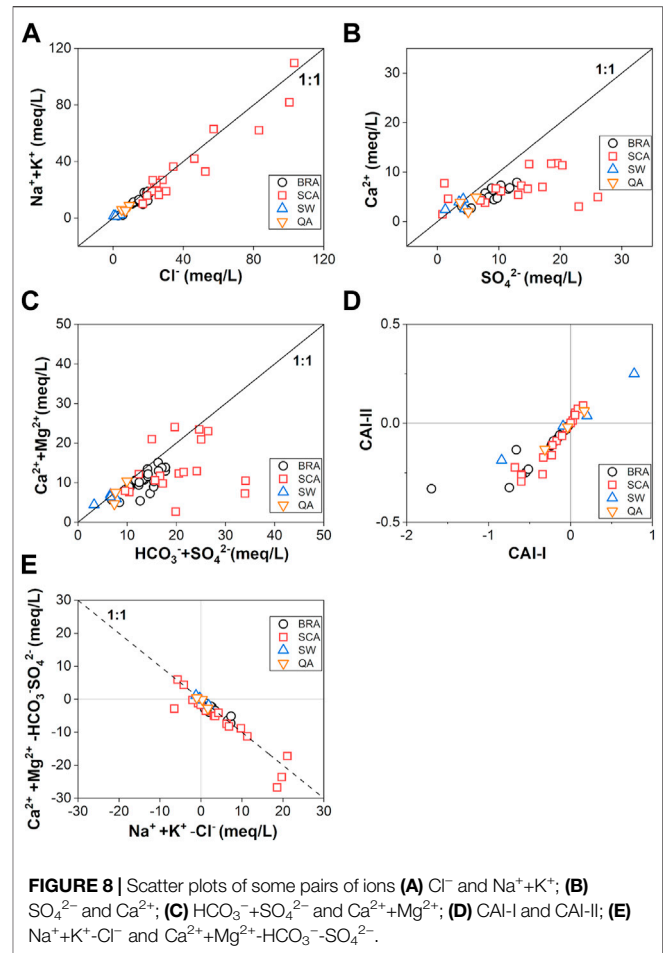
interaction. As a result, the high velocity of the groundwater flow results in low concentrations of ions in BRA.

DISCUSSION

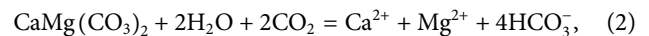
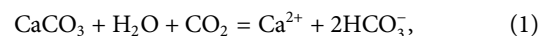
Geogenic Sources of Chemical Compositions in Groundwater

The source of groundwater and the process of hydrogeochemistry can be identified by the ratio coefficient of the major ions (Li et al., 2016). Combined with MSA, more valuable information about the relationship between hydrogeochemical components can be found.

The ideal ratios of Cl and Na would be one, if such ions are released by halite dissolution (Ettazarini, 2005). Meanwhile, because of the close relationship between Na and Cl calculated by MSA, scatter plots of Na and Cl are drawn in **Figure 8A**. Most samples are plotted along the 1:1 line, indicating that the dissolution of halite could be the main hydrogeochemical process in this area. This result is consistent with the principal component analysis, and both refer to the salinity component.



Similar to the dissolution line of halite, carbonate and gypsum dissolution have the decided ratio relationship (Eqs. 1–3).



As the main parameter for calculating hardness, the relationship between Ca and Mg also indicates the hardness component in PCA. Considering the significant correlations between Ca, Mg, and SO_4 , most water samples were below the 1:1 line of gypsum dissolution (**Figure 8B**) and above the 2:1 line of carbonate dissolution (**Figure 8C**), which point toward cation exchange. Therefore, the Schoeller indices (CAI-I and CAI-II) and the relationship between (Na-Cl) and (Ca + Mg- HCO_3^- - SO_4) (**Figures 8D,E**) were employed to verify that the cation exchange is one of the hydrogeochemical processes. CAI-I and CAI-II were calculated according to the following Eqs 4, 5, where ions are expressed in meq/L.

$$\text{CAI-I} = [\text{Cl}^- - (\text{Na}^+ + \text{Cl}^-)] / \text{Cl}^-, \quad (4)$$

$$\text{CAI-II} = [\text{Cl}^- - (\text{Na}^+ + \text{Cl}^-)] / (\text{HCO}_3^- + \text{SO}_4^{2-} + \text{CO}_3^{2-} + \text{NO}_3^-), \quad (5)$$

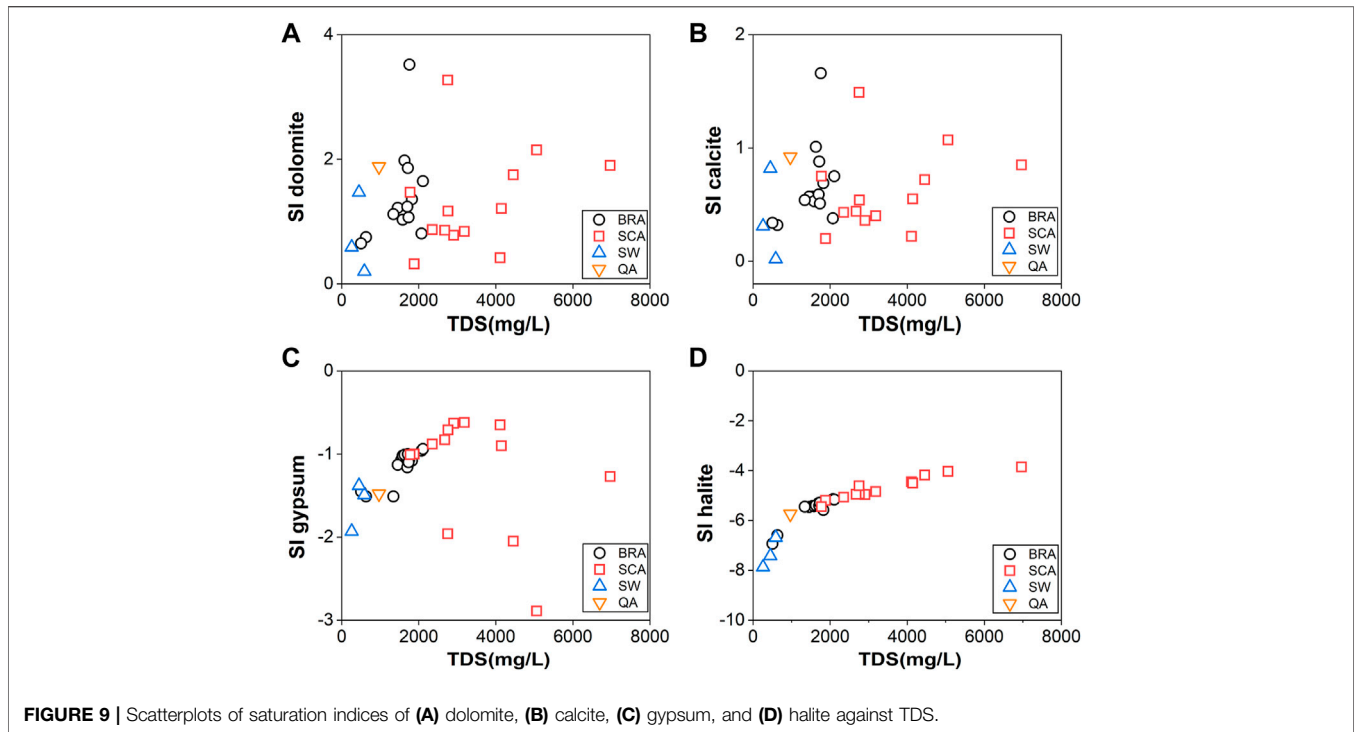


FIGURE 9 | Scatterplots of saturation indices of (A) dolomite, (B) calcite, (C) gypsum, and (D) halite against TDS.

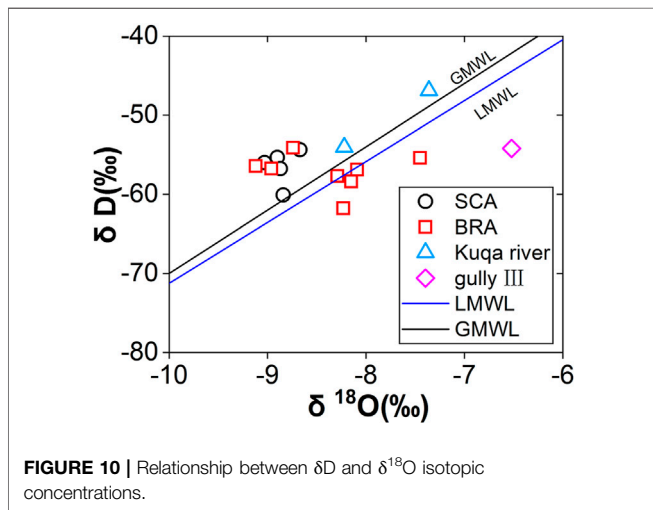


FIGURE 10 | Relationship between δD and δ¹⁸O isotopic concentrations.

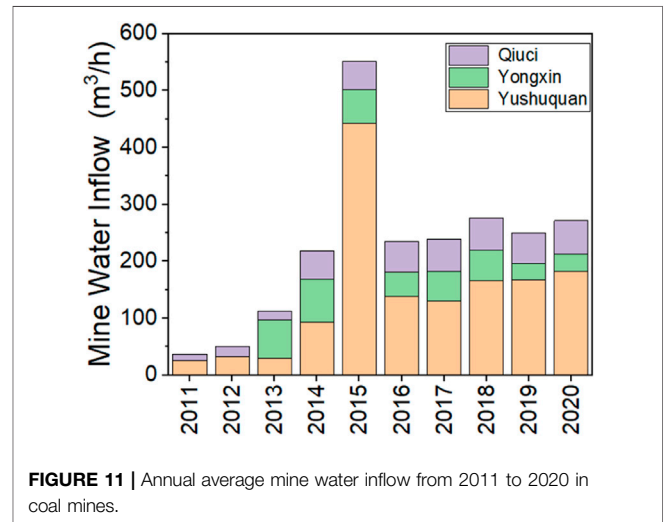


FIGURE 11 | Annual average mine water inflow from 2011 to 2020 in coal mines.

If cation exchange has a significant impact on hydrogeochemical evolution, the water samples should fall in the third quadrant in **Figure 8D** with negative CAI values and linear with a slope of -1 in **Figure 8E** (Fisher and Iii, 1997). Thus, most samples exhibit cation exchange plays an important role in this area. Furthermore, the slightly negative correlation between HCO_3^- and Ca (-0.004 in **Table 2**) indicates the possible dedolomitization process. With the increase in the Ca concentration caused by the dissolution of gypsum, the dissolution of dolomite will also lead to a

decrease in HCO_3^- with the precipitation of calcite. The process could be simplified as follows (Zang et al., 2015).



Therefore, halite, carbonate and gypsum dissolution, cation exchange, and dedolomitization significantly affect the variation of the major cations in the groundwater of the A-ai coalfield.

The saturation index (SI) of minerals can be calculated from the equation: $\text{SI} = \log (K_{\text{IAP}}/K_{\text{SP}})$, where K_{IAP} is the ion activity

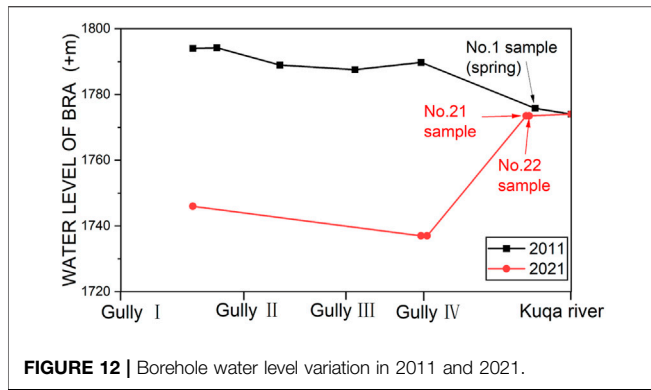


FIGURE 12 | Borehole water level variation in 2011 and 2021.

product for the mineral equilibrium reaction, and K_{SP} is the solubility product. The results of the SI suggest a trend of mineral equilibrium and water–rock interaction, which was calculated by the PHREEQC program and is shown in **Table 1**. The relationship between SI and TDS for each aquifer is shown in **Figure 9**. The halite and gypsum concentrations for all groundwater samples have negative SI values, while a positive trend with TDS can be seen in **Figures 8C,D**. This indicates that the mineral will be continuously weathered by the groundwater and cause increments of TDS. However, it should be noted that water samples from low permeability in SCA have a higher saturation index than those from the high permeability BRA and surface water. In contrast, the SI values of dolomite and calcite from all samples were greater than zero, indicating that these samples were oversaturated with carbonate minerals. The precipitation of calcite and dolomite in groundwater may be related to low rainfall and strong evaporation (Kumar and Singh, 2015).

Origin of Groundwater

Using stable isotopes of δD and $\delta^{18}O$ is an effective method to analyze groundwater circulation and origin (Craig, 1961).

In this study, the local meteoric water line (LMWL) was used as a baseline, where $\delta D = 7.70\delta^{18}O + 5.74$ (Wang and Zhang, 2017). The global meteoric water line (GMWL, $\delta D = 8\delta^{18}O + 10$, Craig, 1961) is also plotted in **Figure 10**. The difference in the slope and intercept of LMWL can reflect the vapor sources and climatic conditions in different regions. Through comparison of the two lines, the slope and intercept of the LMWL (7.70, 5.74) are significantly smaller than those of the GMWL (8, 10), indicating the dry climate and strong evaporation in this area (Wu et al., 2010).

All groundwater samples are distributed close to the GMWL and LMWL, indicating that meteoric origin is the major recharge source. In addition, the deviation of groundwater isotope values from the meteoric waterline may be caused by the secondary evaporation of precipitation before infiltration (Peng et al., 2004). Meanwhile, most SCA water samples deviate significantly from LMWL compared to BRA water samples, indicating that the longer water–rock interaction in SCA than that of BRA. Due to the low flow rate and the long flow path, the surface water from Gully III experienced more intense evaporation and deviated from LMWL more than that from the Kuqa River.

According to the identification method from USGS (Lindsey et al., 2019), the tritium-based age of groundwater could be classified into the modern (post-1950s) and premodern (pre-1950s) thresholds. Groundwater with a tritium content of less than 0.5 TU is classified as premodern groundwater, while larger than 0.5 TU is classified as a modern one. As shown in **Table 1**, the 3H concentrations of water samples from SCA range from 0.28 to 0.39 TU with a mean value of 0.34 TU, indicating that the age of groundwater from SCA is earlier than in the 1950s. In contrast, the 3H concentrations from BRA (ranging from 3.03 to 8.96 TU with a mean value of 5.84) and surface water (ranging from 7.11 to 10.37 TU with a mean value of 8.74) are significantly higher than the threshold. Combined with the results of stable isotopes, one can conclude that the water in BRA is recharged since the 1950s. Furthermore, although the origins of

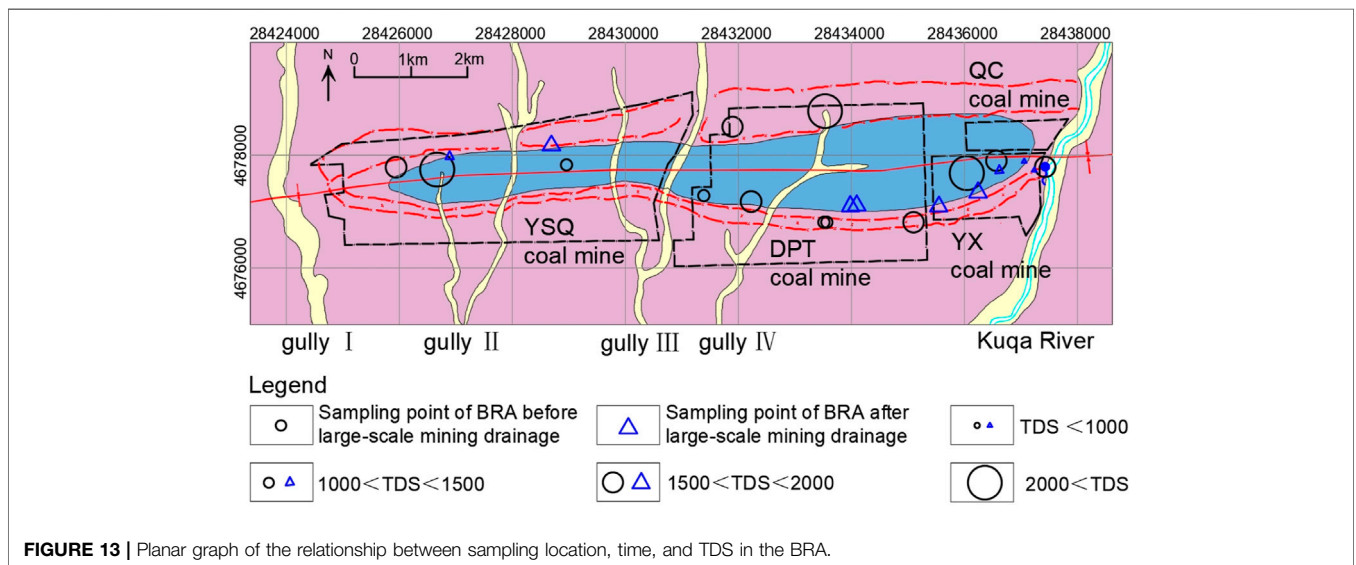
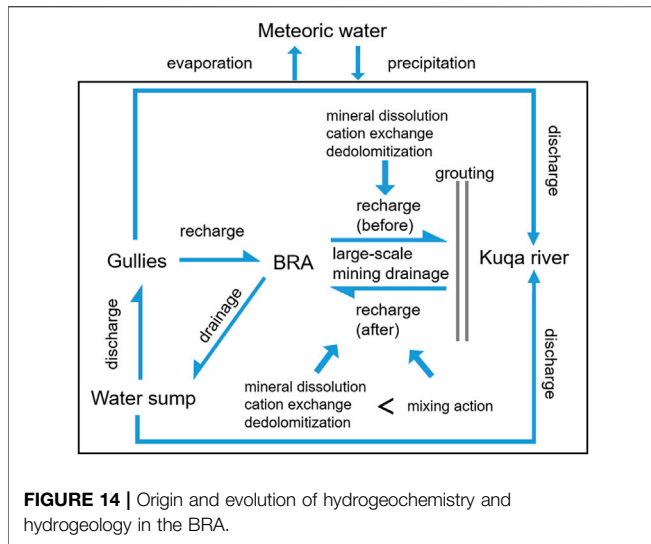


FIGURE 13 | Planar graph of the relationship between sampling location, time, and TDS in the BRA.



groundwater are all from precipitation through rock outcrops, the circulation condition of BRA is better than SCA, which is consistent with the results of stable isotopic of δD and $\delta^{18}O$.

Effect of Large-Scale Mining Drainage on Hydrogeochemistry

According to the previous discussion, BRA is superior to SCA in terms of the recharge conditions, K, and flow velocity. Therefore, BRA is the main aquifer in the A-ai coalfield and has been drained by boreholes during the mining process. With increases in coal production, the average annual mine water inflow also increases (Figure 11), which mainly comes from BRA (it should be noted that because the DPT coal mine has not been produced, only three mines are included). In particular, in the YSQ coal mine, large-scale mining drainage was carried out in 2015, and the spring was cut off in this year. This year is considered to be the start of large-scale mining drainage. Due to the lack of long-term and continuous water level observation data, the water level of BRA boreholes along the syncline in 2011 and 2021 is shown in Figure 12. Under natural conditions or before large-scale mining drainage in 2011, groundwater in BRA flowed from the west to the east and discharged into the Kuqa River. In contrast, after large-scale mining drainage for many years, the water level of BRA declined sharply by almost 50 m. The water level of the Kuqa River is significantly higher than that of BRA and may cause the discharge of the river to the BRA.

In order to further study the influence of water level decline on hydrogeochemical characteristics, the water samples of BRA were divided into two clusters, according to the sampling time (before or after the start year of large-scale mining drainage in 2015), as shown on the planar graph (Figure 13), where the diameter of the circle represents the value of TDS. First, sampling locations near the outcrop area are easier to receive recharge from meteoric water thus with lower TDS. Second, the water chemical types of these two

clusters are different and the concentration of HCO_3 slightly increased in the second cluster, indicating that additional origin or water–rock interaction occurs in these samples. In the YX coal mine area, the TDS of the second cluster samples is significantly lower than the first cluster, and TDS gradually increases from the east to the west. More attention should be paid to samples 21 and 22 from BRA with approximately 300 m away from the Kuqa River. These two samples were collected from underground boreholes in YX coal mine, which have similar hydrogeochemical characteristics and quite a low TDS (630.71 and 505.53 mg/L, respectively). Obviously, the decline of the water level resulted in changes in the groundwater circulation condition. Low mineralization surface water flowed into the BRA through outcrop from the Kuqa River, and thus, this river has transferred from the recharge boundary to the discharge boundary. Therefore, the major hydrogeochemical process of BRA near the Kuqa river is mixing. As drainage continues, this variation will spread more widely.

Comprehensive Analysis and Water Resource Protection

Combined with the aforementioned discussions, the origin and evolution of hydrogeochemistry and hydrogeology in the BRA of the A-ai coalfield is summarized in Figure 14. Before large-scale mining drainage, seasonal flow in gullies of surface water will directly recharge to BRA; then, groundwater flows from the west to the east and recharges to the Kuqa River. During this process, mineral dissolution, such as halite, carbonate and gypsum, cation exchange, and dedolomitization play a pivotal role in the hydrogeochemical evolution. With large-scale mining drainage, the spring is disappearing, and the groundwater in the BRA start receiving recharge from the Kuqa River. At this point, the effect of the mixing action is markedly stronger than in other hydrogeochemical processes. Meanwhile, much groundwater flowed into the coal mine water sump and was discharged to the gullies or the Kuqa River after treatment and purification. Finally, a greater amount of low mineralization surface water will enter into the aquifer. As a result, the hydrogeochemistry of the aquifer will be changed in a wider range. On the other hand, clean and valuable surface water resources would be contaminated continuously in this area.

Drainage is inevitable during the mining process, so obstructing the source of recharge to protect water resources is a better approach. Considering the dry climate and less effect of precipitation, cutting off the flow path from the Kuqa River to the BRA is a preferred method. According to the hydrogeological characteristic of the burnt rock, the high permeability provides a good foundation for grouting. On the east side of the YX and QC coal mine, which is along the Kuqa River, cement could be injected into the BRA through boreholes to construct an underground curtain to effectively separate the Kuqa River and BRA. After that, only limited storage in the BRA and little recharge from precipitation is necessary for drainage. This not only decreases the cost of drainage but also protects the water

resource. More importantly, coal mines in the A-ai coalfield will not be threatened by the water hazards of the BRA and would avoid casualties related to tunnel flooding.

CONCLUSION

In this study, we analyzed the effect of large-scale mining drainage on the regional characteristics of hydrogeochemistry in an arid coalfield by analyzing hydrogeochemical (major ions, ^3H , and stable isotopes of δD and $\delta^{18}\text{O}$) and hydrogeological data (pumping tests, annual average mine water inflow, and water level). The results showed that precipitation is the main recharge source of groundwater and surface water. In addition, the SCA is dominated by the Na-Cl- SO_4 type with higher TDS but has poor permeability and water yield. The significantly low concentrations of ^3H and high mineralization in SCA indicate the old water age and the weak hydraulic connection with other aquifers. In contrast, as the main risk factor for coal mine water hazards, the BRA has a young age and similar water chemical type with SCA but with a lower TDS. Spontaneous combustion of the coal seam caused a remarkable increase in permeability and the good recharge condition caused the strong water yield, which resulted in casualties and tunnel flooding events. Under natural or small-scale mining drainage conditions, groundwater flowed from the west to the east under the water-rock interaction of dissolution of halite, carbonate and gypsum, cation exchange, and dedolomitization, and they were finally discharged to the Kuqa River. After the perennial large-scale mining drainage, the water level of the BRA decreased sharply, causing changes to the hydrogeological condition. Furthermore, the main hydrogeochemical process in the BRA gradually changed from being a water-rock interaction into a mixing action. The influence range will gradually expand with continuous drainage. On the basis of the high permeability of the BRA, we proposed practical advice for the sustainable development and protection of

surface water resources by grouting. By doing so, we could avoid the loss of surface water caused by prolonged drainage.

Similar to other coalfield areas, long-term mining activities have largely destroyed the original groundwater circulation pattern and produced a large amount of acid mine water. The results of this study provided a comprehensive analysis of groundwater evolution for the A-ai coalfield and also could serve as a template for other coalfields in northwest China to enhance the awareness of water resource protection (Huang et al., 2017).

DATA AVAILABILITY STATEMENT

The original contributions presented in the study are included in the article/supplementary material; further inquiries can be directed to the corresponding author.

AUTHOR CONTRIBUTIONS

AK, SZ, WG, and WH contributed to the conception and design of the study. AK, JZ, and XJ organized the database. AK and DS performed the statistical analysis. AK and SZ wrote the first draft of the manuscript. All authors contributed to manuscript revision, read, and approved the submitted version.

FUNDING

This work was financially supported by the Chinese 13th Five-Year Key Research and Development Program (Grant No. 2017YFC0804100).

REFERENCES

- Baboolal, A. A., Knight, J., and Wilson, B. (2018). Petrography and Mineralogy of Pyrometamorphic Combustion Metamorphic Rocks Associated with Spontaneous Oxidation of Lignite Seams of the Erin Formation, Trinidad. *J. S. Am. Earth Sci.* 82, 181–192. doi:10.1016/j.jsames.2018.01.002
- Barzegar, R., Moghaddam, A. A., Tziritis, E., Fakhri, M. S., and Soltani, S. (2017). Identification of Hydrogeochemical Processes and Pollution Sources of Groundwater Resources in the Marand Plain, Northwest of Iran. *Environ. Earth Sci.* 76 (7), 16. doi:10.1007/s12665-017-6612-y
- Carrillo-Rivera, J. J., Varsanyi, I., Kovacs, L., and Cardona, A. (2007). Tracing Groundwater Flow Systems with Hydrogeochemistry in Contrasting Geological Environments. *Water Air Soil Pollut.* 184 (1-4), 77–103. doi:10.1007/s11270-007-9400-6
- Chen, Z., Zhou, X., Du, J., Xie, C., Liu, L., Li, Y., et al. (2015). Hydrochemical Characteristics of Hot Spring Waters in the Kangding District Related to the Lushan Earthquake in Sichuan, China. *Nat. Hazards Earth Syst. Sci.* 15 (6), 1149–1156. doi:10.5194/nhess-15-1149-2015
- Cloutier, V., Lefebvre, R., Therrien, R., and Savard, M. M. (2008). Multivariate Statistical Analysis of Geochemical Data as Indicative of the Hydrogeochemical Evolution of Groundwater in a Sedimentary Rock Aquifer System. *J. Hydrology* 353 (3-4), 294–313. doi:10.1016/j.jhydrol.2008.02.015
- Craig, H. (1961). Isotopic Variations in Meteoric Waters. *Science* 133 (3465), 1702–1703. doi:10.1126/science.133.3465.1702
- Dehghanzadeh, R., Safavy Hir, N., Shamsy Sis, J., and Taghipour, H. (2015). Integrated Assessment of Spatial and Temporal Variations of Groundwater Quality in the Eastern Area of Urmia Salt Lake Basin Using Multivariate Statistical Analysis. *Water Resour. Manage* 29 (4), 1351–1364. doi:10.1007/s11269-014-0877-7
- Dimitrova-Petrova, K., Geris, J., Wilkinson, M. E., Lilly, A., and Soulsby, C. (2020). Using Isotopes to Understand the Evolution of Water Ages in Disturbed Mixed Land-Use Catchments. *Hydrol. Process.* 34 (4), 972–990. doi:10.1002/hyp.13627
- Dong, S. N., Zhou, W. F., and Wang, H. (2021). Introduction to Special Issue on Mine Water Inrushes: Risk Assessment, Mitigation, and Prevention. *Mine Water Environ.* 40 (2), 321–323. doi:10.1007/s10230-021-00782-2
- Emvoutou, H. C., Tandia, B. K., Nkot, S. N. B., Ebonji, R. C. S., Nlend, Y. B., Ekodeck, G. E., et al. (2018). Geologic Factors Controlling Groundwater Chemistry in the Coastal Aquifer System of Douala/Cameroon: Implication for Groundwater System Functioning. *Environ. Earth Sci.* 77 (5), 23. doi:10.1007/s12665-018-7400-z
- Ettazarini, S. (2005). Processes of Water-Rock Interaction in the Turonian Aquifer of Oum Er-Rabia Basin, Morocco. *Environ. Geol.* 49 (2), 293–299. doi:10.1007/s00254-005-0088-x

- Fisher, R. S., and Mullican, III, W. F. (1997). Hydrochemical Evolution of Sodium-Sulfate and Sodium-Chloride Groundwater beneath the Northern Chihuahuan Desert, Trans-Pecos, Texas, USA. *Hydrogeology J.* 5 (2), 4–16. doi:10.1007/s100400050102
- Hao, C.-M., Huang, Y., Ma, D.-J., and Fan, X. (2020). Hydro-geochemistry Evolution in Ordovician Limestone Water Induced by Mountainous Coal Mining: A Case Study from North China. *J. Mt. Sci.* 17 (3), 614–623. doi:10.1007/s11629-019-5485-9
- Huang, L., Liu, C. Y., Yang, L., Zhao, J. F., and Fang, J. J. (2008). Petrologic and REE Geochemical Characters of Burnt Rocks. *Acta Geol. sin.-engl. Ed.* 82 (2), 392–398. doi:10.1111/j.1755-6724.2008.tb00589.x
- Huang, T., Pang, Z., Li, J., Xiang, Y., and Zhao, Z. (2017). Mapping Groundwater Renewability Using Age Data in the Baiyang Alluvial Fan, NW China. *Hydrogeol. J.* 25 (3), 743–755. doi:10.1007/s10040-017-1534-z
- Jia, H., Qian, H., Qu, W., Zheng, L., Feng, W., and Ren, W. (2019). Fluoride Occurrence and Human Health Risk in Drinking Water Wells from Southern Edge of Chinese Loess Plateau. *Int. J. Environ. Res. Public Health* 16 (10), 1683. doi:10.3390/ijerph16101683
- Keita, S., and Zhonghua, T. (2017). The Assessment of Processes Controlling the Spatial Distribution of Hydrogeochemical Groundwater Types in Mali Using Multivariate Statistics. *J. Afr. Earth Sci.* 134, 573–589. doi:10.1016/j.jafrearsci.2017.07.023
- Khanoranga, K., and Khalid, S. (2019). An Assessment of Groundwater Quality for Irrigation and Drinking Purposes Around Brick Kilns in Three Districts of Balochistan Province, Pakistan, through Water Quality Index and Multivariate Statistical Approaches. *J. Geochem. Explor.* 197, 14–26. doi:10.1016/j.gexplo.2018.11.007
- Kruszewski, L., Fabiańska, M. J., Ciesielczuk, J., Segit, T., Orłowski, R., Motyliński, R., et al. (2018). First Multi-Tool Exploration of a Gas-Condensate-Pyrollysate System from the Environment of Burning Coal Mine Heaps: An *In Situ* FTIR and Laboratory GC and PXRD Study Based on Upper Silesian Materials. *Sci. Total Environ.* 640–641, 1044–1071. doi:10.1016/j.scitotenv.2018.05.319
- Kumar, A., and Singh, C. K. (2015). Characterization of Hydrogeochemical Processes and Fluoride Enrichment in Groundwater of South-Western Punjab. *Water Qual. Expo. Health* 7 (3), 373–387.
- Laita, E., Bauluz, B., and Yuste, A. (2019). High-Temperature Mineral Phases Generated in Natural Clinkers by Spontaneous Combustion of Coal. *Minerals* 9 (4), 17. doi:10.3390/min9040213
- Li, X., Jiang, F., Li, L., and Wang, G. (2011). Spatial and Temporal Variability of Precipitation Concentration Index, Concentration Degree and Concentration Period in Xinjiang, China. *Int. J. Climatol.* 31 (11), 1679–1693. doi:10.1002/joc.2181
- Li, P., Zhang, Y., Yang, N., Jing, L., and Yu, P. (2016). Major Ion Chemistry and Quality Assessment of Groundwater in and Around a Mountainous Tourist Town of China. *Expo. Health* 8 (2), 239–252. doi:10.1007/s12403-016-0198-6
- Lindsey, B., Jurgens, B. C., and Belitz, K. (2019). *Tritium as an Indicator of Modern, Mixed, and Premodern Groundwater Age*.
- Liu, L., Zhang, C., He, D., Wei, B., and Li, C. (2011). Chemical Compositions of Detrital Feldspars and Micas within the Late Triassic and Early Jurassic Sequences of Northern Kuqa Basin, Xinjiang and Their Implications to Provenance Tectonics. *Acta Petrol. Sin.* 27 (1), 310–320.
- Liu, F., Zhao, Z., Yang, L., Ma, Y., Xu, Y., Gong, L., et al. (2020). Geochemical Characterization of Shallow Groundwater Using Multivariate Statistical Analysis and Geochemical Modeling in an Irrigated Region along the Upper Yellow River, Northwestern China. *J. Geochem. Explor.* 215, 106565. doi:10.1016/j.gexplo.2020.106565
- Loáiciga, H. A. (2004). Residence Time, Groundwater Age, and Solute Output in Steady-State Groundwater Systems. *Adv. Water Resour.* 27 (7), 681–688. doi:10.1016/j.advwatres.2004.05.004
- Ma, D. Y., Ruan, R. H., Li, Y. D. A., Zhang, L., Wang, X. B., Zi, J. B., et al. (2021). Characteristics of Fine Particle Formation during Combustion of Xinjiang High-Chlorine-Sodium Coal. *Fuel* 297, 10. doi:10.1016/j.fuel.2021.120772
- Meyzonnat, G., Barbecot, F., Alvarado, J. C., Pinti, D. L., Lauzon, J. M., and McCormack, R. (2021). Depth-Sequential Investigation of Major Ions, Delta O-18, Delta H-2 and Delta C-13 in Fractured Aquifers of the St. Lawrence Lowlands (Quebec, Canada) Using Passive Samplers. *Water* 13 (13), 25. doi:10.3390/w13131806
- Nagaraju, A., Thejaswi, A., and Sreedhar, Y. (2016). Assessment of Groundwater Quality of Udayagiri Area, Nellore District, Andhra Pradesh, South India Using Multivariate Statistical Techniques. *Earth Sci. Res. J.* 20 (4), E1–E7. doi:10.15446/esrj.v20n4.54555
- Onifade, M., and Genc, B. (2018). Spontaneous Combustion of Coals and Coal-Shales. *Int. J. Min. Sci. Technol.* 28 (6), 933–940. doi:10.1016/j.ijmst.2018.05.013
- Oren, O., and Sensogut, C. (2010). Spontaneous Combustion Liability of Kutahya (Turkey) Region Lignites. *Energy Sources, Part A Recovery, Util. Environ. Eff.* 32 (10), 877–885. doi:10.1080/15567031003587605
- Peng, H., Mayer, B., Harris, S., and Krouse, H. R. (2004). A 10-yr Record of Stable Isotope Ratios of Hydrogen and Oxygen in Precipitation at Calgary, Alberta, Canada. *Tellus B Chem. Phys. Meteorology* 56 (2), 147–159. doi:10.3402/tellusb.v56i2.16410
- Qiao, W., Li, W., Li, T., Chang, J., and Wang, Q. (2017). Effects of Coal Mining on Shallow Water Resources in Semiarid Regions: A Case Study in the Shennan Mining Area, Shaanxi, China. *Mine Water Environ.* 36 (1), 104–113. doi:10.1007/s10230-016-0414-4
- Qiao, W., Li, W., Zhang, S., and Niu, Y. (2019). Effects of Coal Mining on the Evolution of Groundwater Hydrogeochemistry. *Hydrogeol. J.* 27 (6), 2245–2262. doi:10.1007/s10040-019-01969-2
- Qu, S., Shi, Z. M., Liang, X. Y., Wang, G. C., and Jin, X. M. (2021). Origin and Controlling Factors of Groundwater Chemistry and Quality in the Zhiluo Aquifer System of Northern Ordos Basin, China. *Environ. Earth Sci.* 80 (12), 15. doi:10.1007/s12665-021-09735-y
- Sabit, M., JiangLing, H. U., and Ismail, D. (2008). Climatic Change Characteristics of Kuqa River-Weigan River Delta Oasis during Last 40 Years. *Sci. Geogr. Sin.* 28 (4), 518–524. doi:10.3724/SP.J.1047.2008.00014
- Salameh, E., Toll, M., and Al Raggad, M. (2018). Hydrogeochemical Prospecting for Evaporate and Clay Deposits in Harrat Ash Shaam Basalts, Jordan. *J. Geochem. Explor.* 186, 243–255. doi:10.1016/j.gexplo.2017.12.017
- Shi, B. B., Wang, Z. Y., Liu, P., Zhou, F. B., and Peng, C. Y. (2021). Pozzolanicity Verification of Combustion Metamorphic Rocks from Coalfield Fire Zones in China. *J. Loss Prev. Process Ind.* 69, 7. doi:10.1016/j.jlp.2021.104390
- Shvartsev, S., Shen, Z. L., Sun, Z. X., Wang, G. C., Soldatova, E., and Guseva, N. (2016). Evolution of the Groundwater Chemical Composition in the Poyang Lake Catchment, China. *Environ. Earth Sci.* 75 (18), 1239. doi:10.1007/s12665-016-6065-8
- Singh, C. K., Kumar, A., Shashtri, S., Kumar, A., Kumar, P., and Mallick, J. (2017). Multivariate Statistical Analysis and Geochemical Modeling for Geochemical Assessment of Groundwater of Delhi, India. *J. Geochem. Explor.* 175, 59–71. doi:10.1016/j.gexplo.2017.01.001
- Song, Y., Jiang, B., Mathews, J. P., Yan, G., and Li, F. (2017). Structural Transformations and Hydrocarbon Generation of Low-Rank Coal (Vitrinite) during Slow Heating Pyrolysis. *Fuel Process. Technol.* 167, 535–544. doi:10.1016/j.fuproc.2017.08.003
- Wang, S., and Zhang, M. (2017). SPATIO-TEMPORAL CHARACTERISTICS AND INFLUENCING FACTORS OF STABLE ISOTOPES IN PRECIPITATION ACROSS THE CHINESE TIANSHAN MOUNTAINS. *Quat. Sci.* 37 (5), 1119–1130.
- Wang, J. J., Liang, X., Ma, B., Liu, Y. F., Jin, M. G., Knappett, P. S. K., et al. (2021a). Using Isotopes and Hydrogeochemistry to Characterize Groundwater Flow Systems within Intensively Pumped Aquifers in an Arid Inland Basin, Northwest China. *J. Hydrology* 595, 14. doi:10.1016/j.jhydrol.2021.126048
- Wang, X. J., Di, J. Z., Liang, B., Yang, Y., Dong, Y. R., and Wang, M. X. (2021b). Study on Treatment of Acid Mine Drainage by Nano Zero-Valent Iron Synergistic with SRB Immobilized Particles. *Environ. Eng. Res.* 26 (5), 13. doi:10.4491/eer.2020.333
- Wu, J., Ding, Y., Ye, B., Yang, Q., Zhang, X., and Wang, J. (2010). Spatio-temporal Variation of Stable Isotopes in Precipitation in the Heihe River Basin, Northwestern China. *Environ. Earth Sci.* 61 (6), 1123–1134. doi:10.1007/s12665-009-0432-7
- Xiao, Y., Hao, Q., Zhang, Y., Zhu, Y., Yin, S., Qin, L., et al. (2022a). Investigating Sources, Driving Forces and Potential Health Risks of Nitrate and Fluoride in Groundwater of a Typical Alluvial Fan Plain. *Sci. Total Environ.* 802, 149909. doi:10.1016/j.scitotenv.2021.149909
- Xiao, Y., Liu, K., Hao, Q., Xiao, D., Zhu, Y., Yin, S., et al. (2022b). Hydrogeochemical Insights into the Signatures, Genesis and Sustainable Perspective of Nitrate Enriched Groundwater in the

- Piedmont of Hutuo Watershed, China. *CATENA* 212, 106020. doi:10.1016/j.catena.2022.106020
- Xue, J. K., Shi, L., Wang, H., Ji, Z. K., Shang, H. B., Xu, F., et al. (2021). Water Abundance Evaluation of a Burnt Rock Aquifer Using the AHP and Entropy Weight Method: a Case Study in the Yongxin Coal Mine, China. *Environ. Earth Sci.* 80 (11), 12. doi:10.1007/s12665-021-09703-6
- Xuemei, W., Zhongping, C., Tashpolat, T., and Aijin, G. (2009). Analysis on the Characteristics of Soil Salinization in the Northern Margin of Tarim Basin: A Case Study in the Delta Oasis of Weigan and Kuqa Rivers. *J. Arid Land Resour. Environ.* 23 (9), 134–138.
- Yilmaz, V., and Buyukyildiz, M. (2015). FACTOR ANALYSIS OF SURFACE WATER QUALITY PARAMETERS FOR THE RIVERS OF TURKEY. *Fresenius Environ. Bull.* 24 (1), 113–123.
- Yuan, Y., Liu, Z. H., Zhu, C., Yuan, C. F., and Wang, S. Z. (2019). The Effect of Burnt Rock on Inclined Shaft in Shallow Coal Seam and its Control Technology. *Energy Sci. Eng.* 7 (5), 1882–1895. doi:10.1002/ese3.398
- Zang, H., Zheng, X., Jia, Z., Chen, J., and Qin, Z. (2015). The Impact of Hydrogeochemical Processes on Karst Groundwater Quality in Arid and Semiarid Area: a Case Study in the Liulin Spring Area, North China. *Arab. J. Geosci.* 8 (9), 6507–6519. doi:10.1007/s12517-014-1679-1
- Zeng, Q., Shen, L., and Yang, J. (2020). Potential Impacts of Mining of Super-thick Coal Seam on the Local Environment in Arid Eastern Junggar Coalfield, Xinjiang Region, China. *Environ. Earth Sci.* 79 (4), 15. doi:10.1007/s12665-020-8806-y
- Zhang, J. Y., Guo, L. W., Gong, J. L., Zhu, L. Q., and Gong, X. M. (2007). *Analysis on Impacting the Soil Environment of the Underground Coal Mining*. Jiaozuo, PEOPLES R CHINA: Science Press Beijing, 1966–1969.
- Zhang, Y., Zhang, X. Q., Hower, J. C., and Hu, S. R. (2020). Mineralogical and Geochemical Characteristics of Pyrometamorphic Rocks Induced by Coal Fires in Junggar Basin, Xinjiang, China. *J. Geochem. Explor.* 213, 11. doi:10.1016/j.jgexplo.2020.106511
- Zhang, J., Chen, L. W., Hou, X. W., Lin, M. L., Ren, X. X., Li, J., et al. (2021). Multi-isotopes and Hydrochemistry Combined to Reveal the Major Factors Affecting Carboniferous Groundwater Evolution in the Huaibei Coalfield, North China. *Sci. Total Environ.* 791, 148420. doi:10.1016/j.scitotenv.2021.148420

Conflict of Interest: The authors declare that the research was conducted in the absence of any commercial or financial relationships that could be construed as a potential conflict of interest.

Publisher's Note: All claims expressed in this article are solely those of the authors and do not necessarily represent those of their affiliated organizations, or those of the publisher, the editors, and the reviewers. Any product that may be evaluated in this article, or claim that may be made by its manufacturer, is not guaranteed or endorsed by the publisher.

Copyright © 2022 Luo, Wang, Dong, Wang, Shi, Ji and Xue. This is an open-access article distributed under the terms of the Creative Commons Attribution License (CC BY). The use, distribution or reproduction in other forums is permitted, provided the original author(s) and the copyright owner(s) are credited and that the original publication in this journal is cited, in accordance with accepted academic practice. No use, distribution or reproduction is permitted which does not comply with these terms.